inorganics

MDPI

Article

Preparation of Ca-Mg Double-Doped Mesoporous Silica Nanoparticles and Their Drug-Loading and Drug-Releasing Properties

Qian Zhang [1], Jiamin Huang [1], Chao Liu [2], Ruihua Chen [3], Tao Jiang [3], Yusufu Hailili [1], Telieke Bahetibieke [1], Xiaohui Tang [4,*] and Mei Wang [1,5,6,*]

[1] School of Pharmacy, Xinjiang Medical University, Urumqi 830011, China; zhangqianxjmu@163.com (Q.Z.); woahjmjy@163.com (J.H.); 2790610460@163.com (Y.H.); 3549415558@163.com (T.B.)
[2] School of Medical Engineering and Technology, Xinjiang Medical University, Urumqi 830011, China; cliu20@sohu.con
[3] Animal Centre, Xinjiang Medical University, Urumqi 830011, China; xjchenrh@xjmu.edu.cn (R.C.); 13579977272@163.com (T.J.)
[4] Central Laboratory, Xinjiang Medical University, Urumqi 830011, China
[5] Xinjiang Key Laboratory of Natural Medicines Active Components and Drug Release Technology, Xinjiang Medical University, Urumqi 830011, China
[6] Engineering Research Center of Xinjiang and Central Asian Medicine Resources, Ministry of Education, Urumqi 830011, China
* Correspondence: tangxh0429@163.com (X.T.); meiwang@xjmu.edu.cn (M.W.)

Abstract: Breast cancer is a common clinical malignant tumor that seriously threatens women's physical and mental health. Chemotherapy, as the first choice of breast cancer treatment, has limited its application in the clinic due to problems of poor stability, short half-life, and serious toxic side effects. With the emergence of nanotechnology, inorganic materials to prepare mesoporous silica nanoparticles (MSNs) have been widely used in anti-tumor drug carriers. However, their slow degradation rate limits their application in the biomedical field. Therefore, developing low-toxicity MSNs with good biocompatibility, biodegradability, and rapid release at the tumor site is a key scientific issue to be addressed. Here, we prepared DOX-loaded Ca-Mg-doped MSNs by electrostatic adsorption to obtain Ca-Mg@DOX@MSNs with suitable particle sizes and zeta potential, and the incorporation of calcium and magnesium also led to an increase in the degradation rate under acidic conditions and an accelerated release, which reduced the toxicity of DOX and promoted cellular uptake with good anti-tumor effects. This study provides a new idea for the clinical treatment of breast cancer.

Keywords: Ca-Mg double-doped mesoporous silica; Doxorubicin; nanoparticles; breast cancer

Academic Editor: Nabanita Saikia

Received: 3 December 2024
Revised: 31 December 2024
Accepted: 2 January 2025
Published: 4 January 2025

Citation: Zhang, Q.; Huang, J.; Liu, C.; Chen, R.; Jiang, T.; Hailili, Y.; Bahetibieke, T.; Tang, X.; Wang, M. Preparation of Ca-Mg Double-Doped Mesoporous Silica Nanoparticles and Their Drug-Loading and Drug-Releasing Properties. *Inorganics* **2025**, *13*, 12. https://doi.org/10.3390/inorganics13010012

1. Introduction

As a significant global public health problem, cancer is currently one of the diseases with the highest morbidity and mortality rates in the world; it will be the most significant obstacle to the growth of life expectancy of the world population in the 21st century [1–3]. According to the World Cancer Report, the annual number of new cancer cases worldwide is expected to increase from 18 million in 2018 to 27 million in 2040, which is a 50% rise [4]. Among them, breast cancer is the most common clinical malignancy, which seriously threatens women's physical and mental health. According to statistics, the incidence rate of female breast cancer has now exceeded that of lung cancer, becoming the leading cause of global cancer incidence in recent years, accounting for 11.7% of all global cancer cases and

6.9% of total cancer deaths [1]. Current clinical treatments for breast cancer mainly include surgery, radiotherapy, chemotherapy, endocrine therapy, molecular targeted therapy, and immunotherapy [5–9]. Chemotherapy, as the first choice of treatment for breast cancer, has been limited in clinical applications due to the disadvantages of poor stability, short half-life, and the lack of tissue specificity of chemotherapeutic drugs [10,11]. In addition to this, it has also been shown that chemotherapy can lead to complications, such as anthracycline-induced cardiotoxicity [12]. The emergence of nanotechnology provides a powerful tool for effective delivery, responsive release, and reductions in the toxicity of chemotherapeutic drugs [13,14]. Among them, inorganic nanoparticles can be applied to the fields of catalysis and environmental protection [15,16], in addition to their use as drug carriers to deliver anti-tumor medications to the target site and achieve the controlled release of drugs in response to specific internal stimuli in the tumor microenvironment [17–20].

Silica nanoparticles (SiO_2 NPs), the most prevalent inorganic nanoparticles, are widely used in biomedical applications [21,22]. There are two main types of SiO_2 NPs: non-porous and mesoporous silica nanoparticles (MSNs), in which the enormous specific surface area, the ordered and tunable pore size, and the easily modifiable surface of MSNs [23] have led to better applications in the field of anti-tumor drug carriers [24–28]. However, pure silica degrades very slowly due to its stable network structure, which limits its biomedical applications [29,30]. Therefore, the preparation of degradable mesoporous silica drug carriers is significant. In addition, the pores and surface of SiO_2 NPs contain silica hydroxyl (Si-OH) groups that make their zeta potential very damaging, and positively charged drugs can be readily adsorbed to the pores and surface of SiO_2 NPs by electrostatic solid interaction [31], which also lays the foundation for the successful loading of Doxorubicin (DOX).

Recently, in order to overcome the incomplete drug release and toxic bioaccumulation phenomenon of MSNs, researchers have proposed methodological strategies, such as reconfiguring silica nanoparticle structures by organic–inorganic hybridization and metal ion doping [32], to improve the biodegradation properties of MSNs. Academician Shi Jianlin's group at the Shanghai Institute of Silicate Research prepared MSNs doped with manganese ions and organic fragments by sol–gel and hydrothermal methods [33], respectively, successfully achieved the rapid degradation of MSNs in the tumor microenvironment (TME), and also significantly improved the therapeutic effect and the resolution of MRI-weighted images. Aizheng Chen's group at Huaqiao University prepared copper and iron double-doped MSNs by the solvothermal method [34], which achieved the specific biodegradation of MSNs under microacidic conditions. The therapeutic effect of Cu and Fe double-doped drug-carrying MSNs was also superior to that of other types of drug-carrying MSNs. In addition, the intracellular reactive oxygen species level was increased by the Fenton-like reaction catalyzed by Fe and Cu ions. The killing power of the tumor cells was significantly improved with the help of photodynamic therapy, which further enhanced the tumor's therapeutic effect. However, this kind of metal-doped MSN will release many metal ions in the body or the cells during descending explanatory drugs, and the released Mn, Cu, and Fe will cause potential hazards to the human body at higher concentrations. Therefore, it is essential to dope non-toxic and crucial elements in MSN carriers.

In addition, the insufficient intracellular drug release from nanoparticles reduces the amount of anticancer drug that actually reaches the cancer cells, which not only hinders the efficacy of cancer chemotherapy but also induces toxic side effects in vivo. Therefore, the development of low-toxicity MSNs with good biocompatibility, biodegradability, and rapid release at the tumor site is a critical scientific issue that needs to be solved [35]. Ca and Mg are essential minerals in the human body, playing crucial roles in various physiological processes [33]. Ca is primarily involved in the formation and maintenance of bones, nerve transmission, and muscle contraction. In contrast, Mg, as an important

mineral, is widely involved in enzymatic reactions within the body, particularly in energy metabolism, DNA synthesis, protein synthesis, and cellular function regulation. Mg acts as a cofactor for numerous enzymes, regulating intracellular Ca concentrations and supporting normal cellular metabolism and function. Compared with elemental Si, Ca^{2+} reacts more easily with Si-OH to form Si-O-Ca, obtaining the O-Ca bond, which is less stable than the Si-O bond [36], while Mg^{2+} replaces part of the Si in Si-O-Si to form Mg-O-Si. The acid-responsive Mg-O bond obtained combines the advantages of both substances and synergistically exerts an accelerated biodegradation effect on MSNs. The synergistic effects of Ca and Mg not only optimize the performance of MSNs but also improve their prospects in biomedical applications. By adjusting the ratio of these two elements, precise material design can be achieved, facilitating accelerated biodegradation and enhancing their application in the biomedical field.

Doxorubicin (DOX) belongs to the anthracycline glycoside class of drugs and is a commonly used clinical cycle non-specific anti-tumor drug [37]. It kills tumor cells of various growth cycles, but the obvious toxic side effects make its clinical application severely limited. Therefore, in order to promote the further application of DOX in the clinic, exploring a novel therapeutic strategy that can reduce the toxic side effects of DOX [38] while preserving its tumor tissue-killing effect has become a hot issue in breast cancer treatment.

Given this, in this study, DOX was used as a model drug. It was proposed that the Ca-O and Mg-O bonds, which are unstable under acidic conditions, were formed in MSNs by doping the essential Ca-Mg elements in MSNs (Scheme 1). It was proposed to increase the biodegradation rate and drug release rate of MSNs under acidic conditions to make the Ca-Mg-doped MSNs have a higher drug release and drug loading rate in the tumor microenvironment and to promote the killing effect of DOX on tumor cells and exert the excellent performance of reducing the toxicity of DOX at the same time.

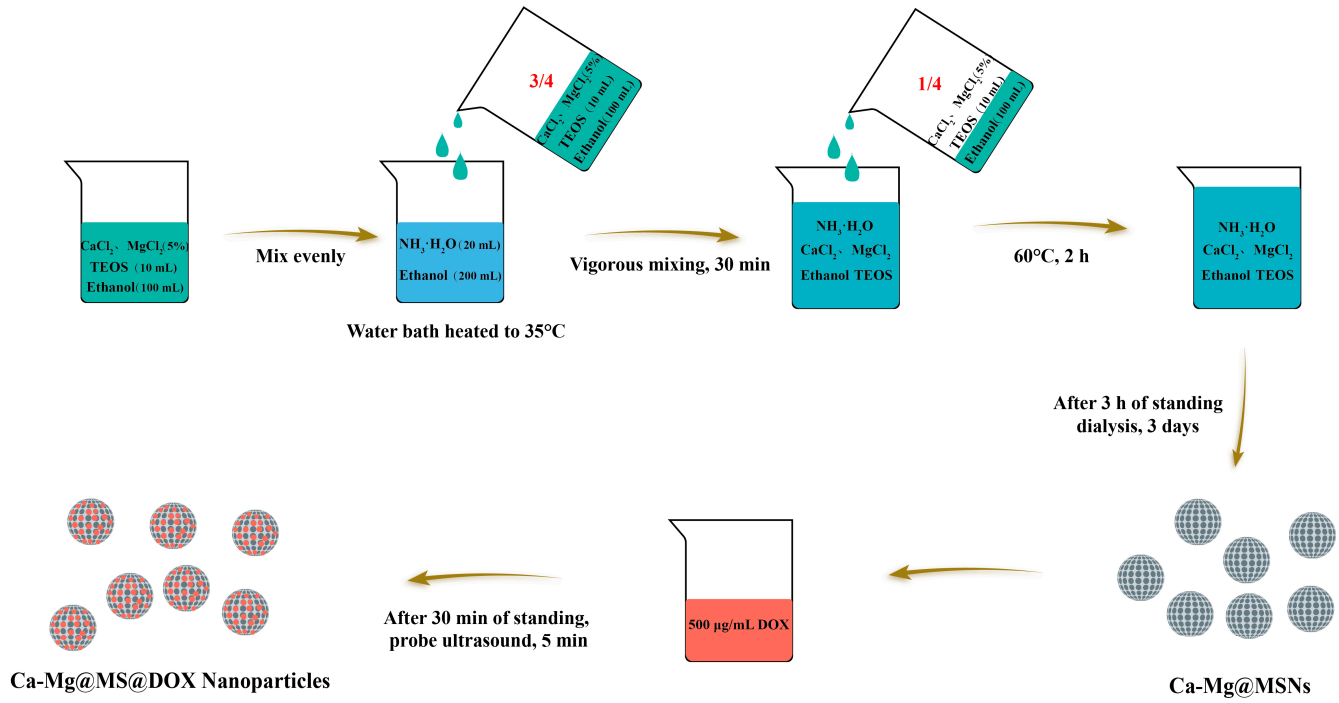

Scheme 1. Schematic illustration of Ca-Mg@DOX@MSNs preparation process.

2. Results

2.1. Characterization of Ca-Mg@MSNs

The MSN subs were dispersed in different concentrations of $CaCl_2$ and $MgCl_2$ solutions, keeping Ca^{2+}:Mg^{2+} = 1:1, and determined the particle size, the PDI, and potential. The results are shown in Figure 1a. The particle sizes of Ca-Mg@MSNs in different concentrations of $CaCl_2$ and $MgCl_2$ solutions were around 200 nm and negatively charged, and the PDI was more significant than 3%. The dispersion was reduced when the concentration of $CaCl_2$ and $MgCl_2$ solutions was more significant than 5%. Therefore, the concentration of $CaCl_2$ and $MgCl_2$ was determined to be 5%.

Ca-Mg@MSNs were prepared with a 5% $CaCl_2$ and $MgCl_2$ concentration. The morphology of MSNs and Ca-Mg@MSNs was observed by scanning electron microscopy; from the results, we can see that the MSNs are regularly spherical-shaped, while Ca-Mg@MSNs are irregularly spherical, which is due to the fact that Mg^{2+} and Ca^{2+} can replace some of the Si in Si-O-Si to form Si-O-M (M = calcium, magnesium), which leads to the morphology change, while, at the same time, it also imparts Ca-Mg@MSN new properties [39,40].

The elemental EDX mapping of scanning electron microscopy was used to observe the content and distribution of $CaCl_2$ and $MgCl_2$. It can be seen from Figure 1d that Ca and Mg elements are indeed present in the Ca-Mg@MSNs, which were successfully synthesized with a uniform distribution of elements, with the content of Ca being 2.92% and that of Mg being 1.19%.

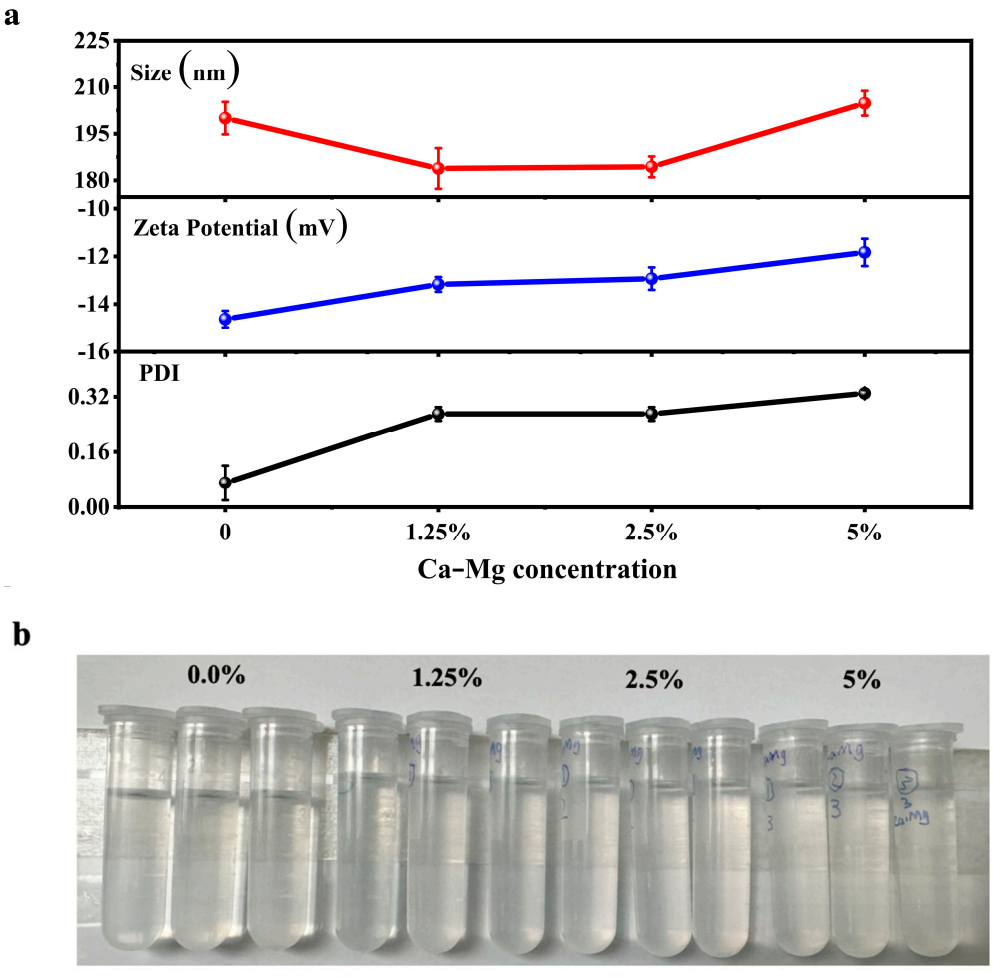

Figure 1. *Cont.*

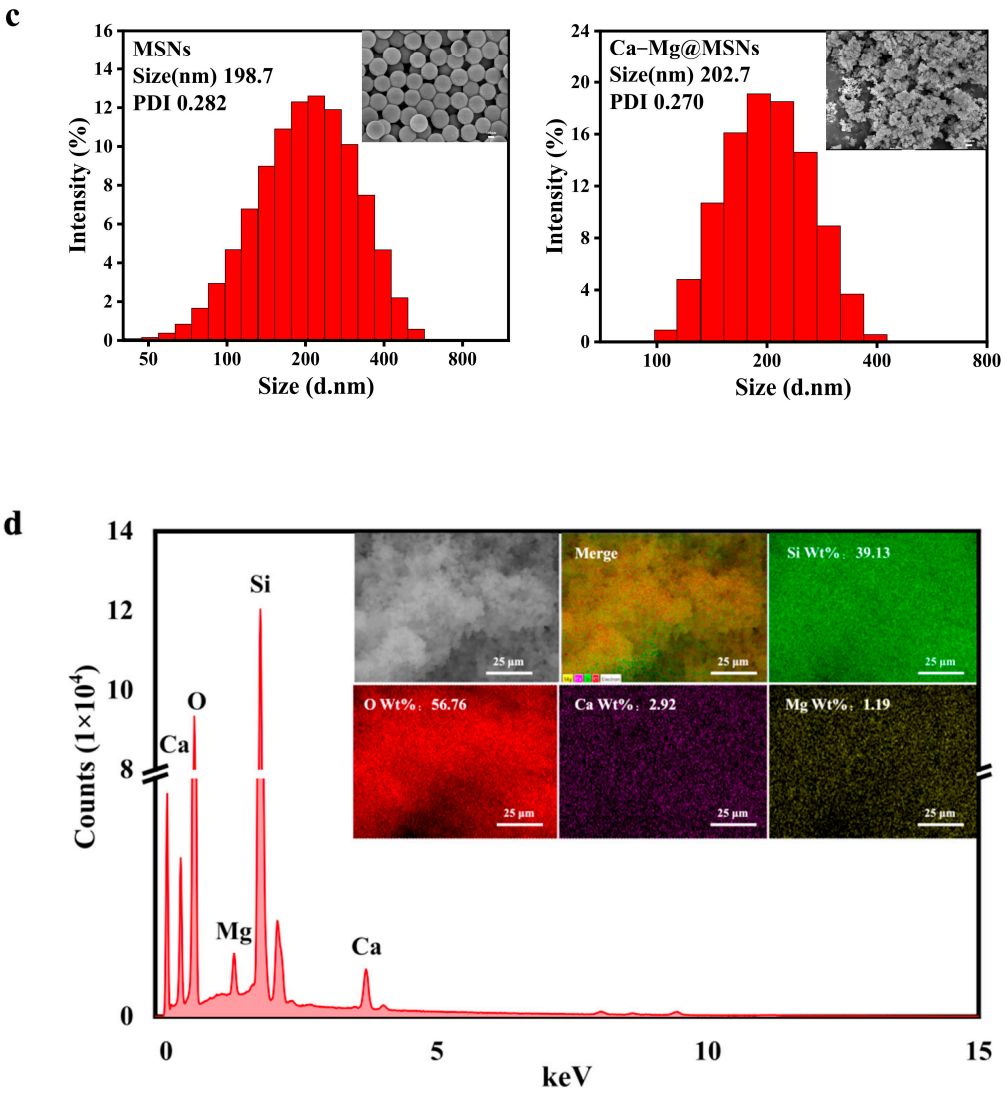

Figure 1. Preparation and characterization of Ca-Mg@MSNs: (**a**) Particle size, PDI, and potential of MSNs with different $CaCl_2$ and $MgCl_2$ concentrations. (**b**) Appearance of MSNs with different $CaCl_2$ and $MgCl_2$ concentrations. (**c**) Particle size, PDI, and morphology of MSNs and Ca-Mg@MSNs. (**d**) Elemental distribution of Ca-Mg@MSNs.

2.2. Characterization of DOX@MSNs and Ca-Mg@DOX@MSNs

2.2.1. Specific Surface Area and Pore Size Analysis (BET)

The specific surface area and the pore size distribution are determined by the BET method and BJH model, respectively. The results are shown in Figure 2a. Both MSNs and Ca-Mg@MSNs had typical type IV isotherms and H3 hysteresis lines, which prove that both materials have the structural characteristics of mesoporous materials, the specific surface areas of 159.07 m^2/g and 32.09 m^2/g, respectively, the mesoporous pore volumes of 0.85 cm^3/g and 0.14 cm^3/g, respectively, and average pore sizes of 23.85 nm and 29.73 nm. In comparison, it can be seen that the BET surface area of Ca-Mg@MSNs decreased, and the pore size increased, indicating that the Ca-Mg@MSNs samples have a complex porous structure. The large size of the pores makes it suitable for high drug-loading efficiency, which also lays a solid foundation for the further loading of DOX.

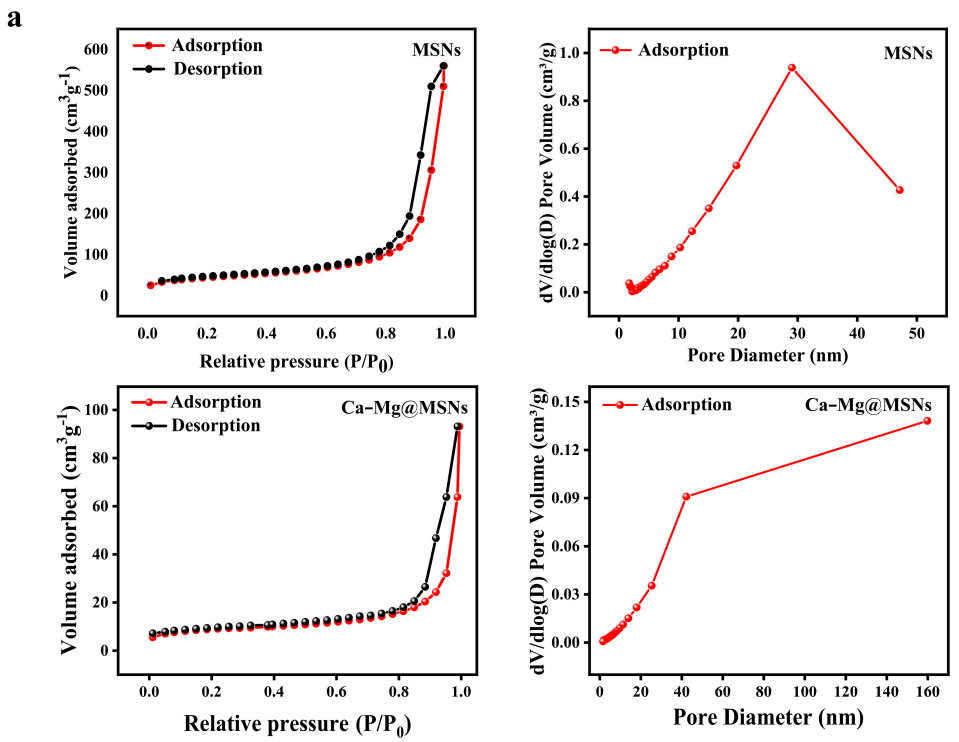

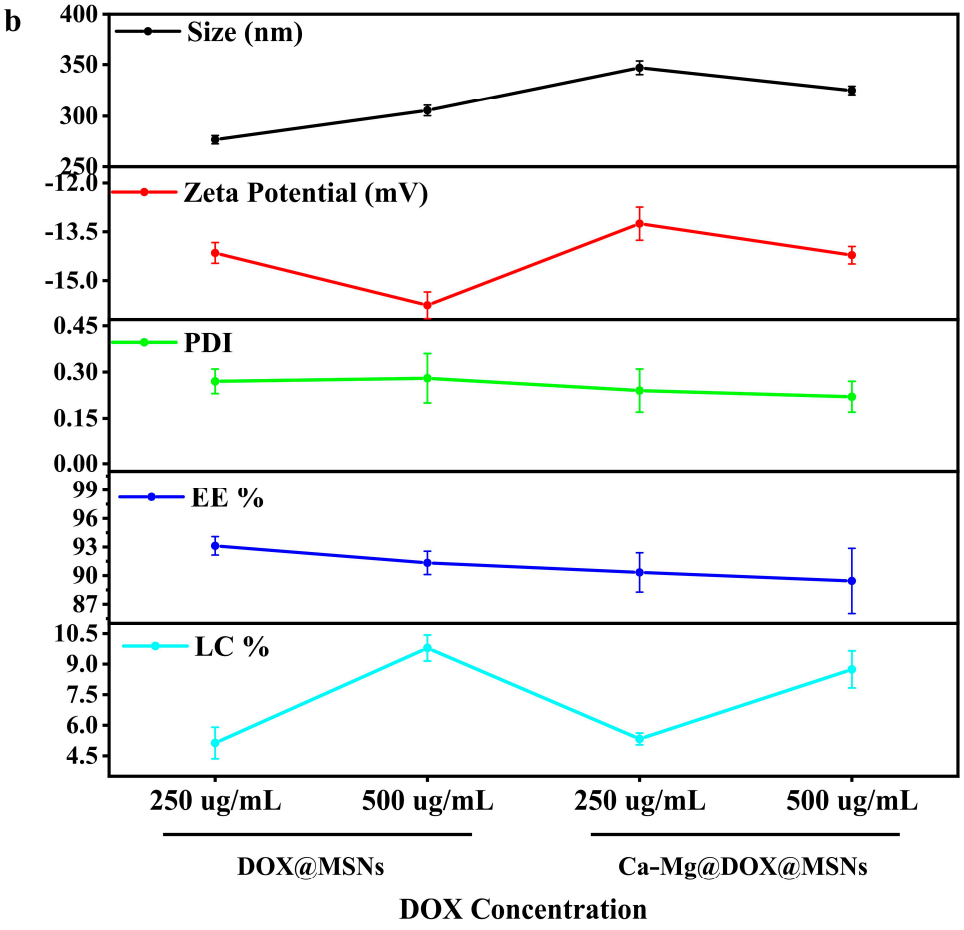

Figure 2. *Cont.*

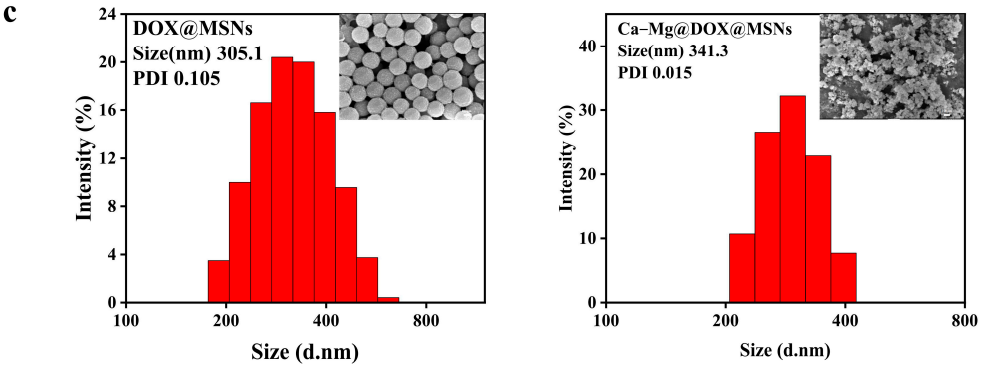

Figure 2. Preparation and characterization of Ca-Mg@DOX@MSNs: (**a**) Results of the BET experiment. (**b**) The particle size, PDI, potential, encapsulation efficiency (%), and loading capacity (%) of DOX@MSNs and Ca-MgDOX@MSNs with different DOX concentrations. (**c**) The particle size, PDI, and morphology of DOX@MSNs and Ca-MgDOX@MSNs.

2.2.2. Determination of Particle Size, Potential, PDI, Drug Loading and Encapsulation Efficiency

MSNs and Ca-Mg@MSNs with different concentrations of DOX were prepared. DOX@MSNs and Ca-Mg@DOX@MSNs had particle sizes of about 200–300 nm, which were negatively charged, and the presence of the electrostatic repulsive force made the prepared nanocarriers more stable and able to be stored for a longer time. It provides the experimental basis for the subsequent in vivo and ex vivo experiments and the regular use of each group of nanoparticles. The encapsulation efficiency was greater than 90%, and the drug loading capacity was more significant than 5%. It lays the foundation for the subsequent exertion of excellent anti-tumor effects (Figure 2b).

Observing the morphology of DOX@MSNs and Ca-Mg@DOX@MSNs by scanning electron microscopy is one of the essential ways of characterization, which can present the results intuitively, objectively, and realistically. From the results, we can see that the distribution of the prepared groups of nanocarriers is uniform, the MSN sub is a regular spherical shape, and the surface of the MSN sphere becomes non-smooth after adding DOX, which proves that DOX is successfully loaded on the surface of MSNs (Figure 2c).

2.3. Release of Ca-Mg@DOX@MSNs

2.3.1. Calculated Results of Molecular Dynamic Simulations of Ca-Mg@DOX@MSNs

Molecular dynamic simulation can be used to study intermolecular interactions and physicochemical properties on the atomic scale, which is of high significance as a guide in the study of the structure and properties of novel mesoporous silica. In molecular dynamic simulation, the magnitude of free energy can reflect the stability of molecules and the strength of interactions under specific conditions. Specifically, the smaller the free energy, the more stable the system is and the stronger the interactions; conversely, the larger the free energy, the more unstable the system is and the weaker the interactions. From Figure 3a, it can be seen that the free energy of the system becomes larger after doping calcium and magnesium, and the free energy of the Ca_2Mg_2@MSNs group is the largest, which indicates that the stability of the MSN system decreases after doping calcium and magnesium and shows a trend of gradual decrease with the increase in theincrease of the amount of calcium and magnesium doped, which also predicts that the doping of calcium and magnesium can improve the degradation rate of MSNs to increase the release of the loaded drug. The cumulative release rate will be examined subsequently to verify the simulation results.

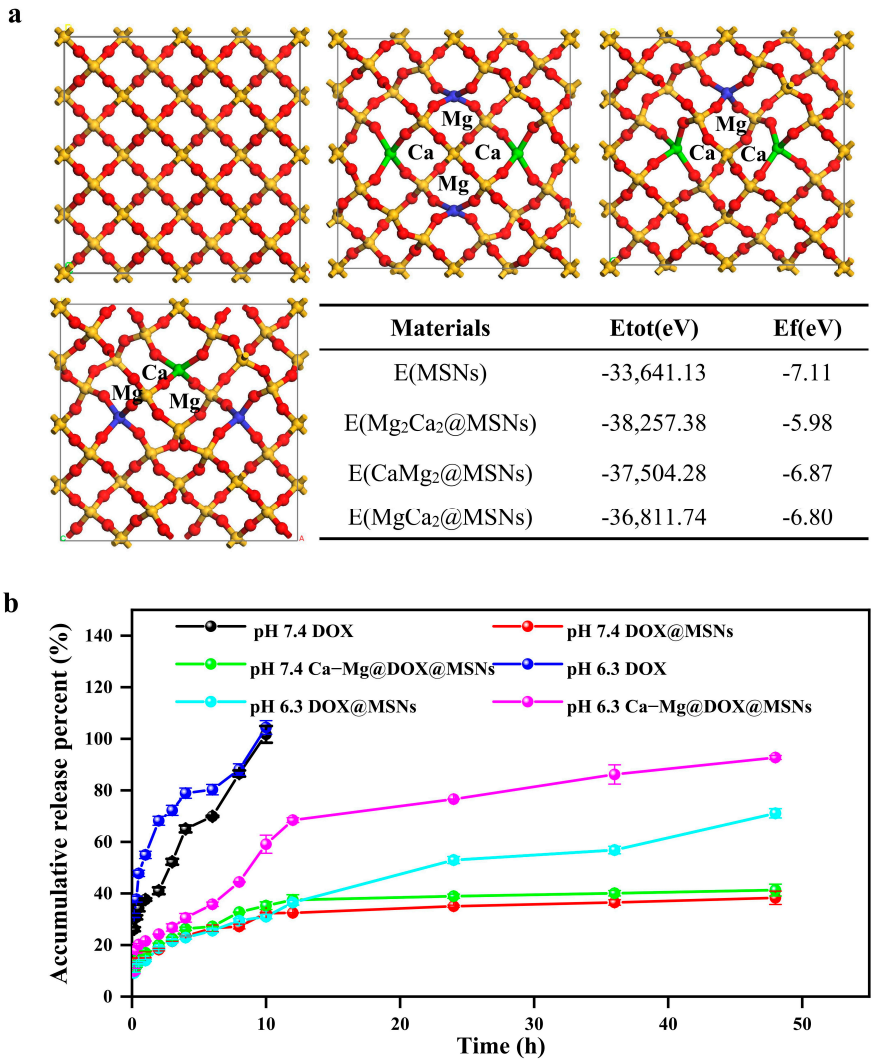

Materials	Etot(eV)	Ef(eV)
E(MSNs)	-33,641.13	-7.11
E(Mg_2Ca_2@MSNs)	-38,257.38	-5.98
E($CaMg_2$@MSNs)	-37,504.28	-6.87
E($MgCa_2$@MSNs)	-36,811.74	-6.80

Figure 3. Release of Ca-Mg@DOX@MSNs: (**a**) Calculated results of molecular dynamic simulations of Ca-Mg@DOX@MSNs. (**b**) Cumulative release of Ca-Mg@DOX@MSNs.

2.3.2. Cumulative Release of Ca-Mg@DOX@MSNs

The drug's ability in the nanoparticles to be released sustainably is a critical factor in achieving therapeutic effects. In this experiment, the in vitro release was investigated using the positive dynamic dialysis method. The results are shown in Figure 3b; free DOX could be rapidly released in 10 h under different pH conditions, while the release rate of the Ca-Mg@DOX@MSNs is higher than that of DOX@MSN under both pH 7.4 and pH 6.3. This result is consistent with molecular dynamic simulations, as calcium and magnesium doping decreases the stability of the MSN system, which in turn accelerates the rate of drug release. We also found that Ca-Mg@DOX@MSNs were relatively stable in the PBS solution at pH 7.4, with less than 50% release in 48 h, while the release rate was significantly increased to 92.73 ± 0.76% under acidic conditions at pH 6.3. This result also indicates that the prepared nanoparticles release better in the tumor environment than in normal tissues, which can exert a better anti-tumor effect. The results of fitting the cumulative release and time (Tables 1 and 2) showed that MSNs, DOX@MSNs, and Ca-Mg@DOX@MSNs conformed to the first-order kinetic model, Weibull's distribution function, and Higuchi's model, respectively, at pH 7.4, and MSNs conformed to the Higuchi's model at pH 6.3. In contrast, DOX@MSNs conformed to Higuchi's model, and DOX@MSNs were more consistent with the mono-exponential and first-order kinetic models. In comparison, Ca-Mg@DOX@MSNs were more consistent with the first-order kinetic model.

Table 1. Dissolution curve fitting of DOX@MSNs and Ca-Mg@DOX@MSNs in pH 7.4.

Model	DOX	r	DOX@MSNs	r	Ca-Mg @DOX@MSNs	r
Single index model	$lg(y\infty - y) = lgy\infty - 0.195t/2.303$	0.976	$lg(y\infty - y) = lgy\infty - 0.007t/2.303$	0.848	$lg(y\infty - y) = lgy\infty + 0.007t/2.303$	0.683
Zero–order kinetic	$Q = 7.3056t + 28.983$	0.993	$Q = 0.523t + 18.896$	0.825	$Q = 0.5902t + 20.293$	0.795
First–order kinetics	$\ln(1 - Q) = -0.195t - 0.2463$	0.976	$\ln(1 - Q) = -0.0072t - 0.2112$	0.848	$\ln(1 - Q) = -0.0083t - 0.2305$	0.819
Ritger–Peppas	$M\infty/Mt = 0.415t^{0.312}$	0.965	$M\infty/Mt = 0.157t^{0.2392}$	0.844	$M\infty/Mt = 0.171t^{0.2642}$	0.952
Weibull distribution function	$\ln(1/(1 - Q)) = 0.3361\ln t + 0.6602$	0.831	$\ln(1/(1 - Q)) = 0.0757\ln t + 0.1731$	0.913	$\ln(1/(1 - Q)) = 0.0834\ln t + 0.2106$	0.976
Higuchi	$Q = 1.366t^{1/2}$	0.966	$Q = 1.270t^{1/2}$	0.844	$Q = 1.302t^{1/2}$	0.985

Table 2. Dissolution curve fitting of DOX@MSNs and Ca-Mg@DOX@MSNs in pH 6.3.

Model	DOX	r	DOX@MSNs	r	Ca-Mg @DOX@MSNs	r
Single index model	$lg(y\infty - y) = lgy\infty - 0.206t/2.303$	0.968	$lg(y\infty - y) = lgy\infty - 0.022t/2.303$	0.991	$lg(y\infty - y) = lgy\infty + 0.010t/2.303$	0.768
Zero–order kinetic	$Q = 6.2226t + 44.642$	0.932	$Q = 1.2312t + 16.032$	0.973	$Q = 1.715t + 24.906$	0.918
First–order kinetics	$\ln(1 - Q) = -0.2066t - 0.5414$	0.968	$\ln(1 - Q) = -0.0222t - 0.1499$	0.991	$\ln(11 - Q) = -0.0512t - 0.2081$	0.989
Ritger–Peppas	$M\infty/Mt = 0.535t^{0.2684}$	0.99	$M\infty/Mt = 0.140t^{0.3691}$	0.906	$M\infty/Mt = 0.217t^{0.3745}$	0.974
Weibull distribution function	$\ln(1/(1 - Q)) = 0.4169\ln t + 0.957$	0.966	$\ln(1/(1 - Q)) = 0.185\ln t + 0.1078$	0.845	$\ln(1/(1 - Q)) = 0.364\ln t + 0.2856$	0.837
Higuchi	$Q = 1.308t^{1/2}$	0.991	$Q = 1.411t^{1/2}$	0.985	$Q = 1.454t^{1/2}$	0.975

2.4. Safety Evaluation of Ca-Mg@DOX@MSNs

Nanoparticles have the danger of hemolysis, platelet aggregation, or blood coagulation; hemolysis experiments of medical materials, cytotoxicity of the antecedent experiments, and the necessary characterization of blood-contacting materials in the biocompatibility characterization of this piece have a unique and vital position. The results of hemolysis experiments showed that free DOX (30 μg/mL) had a hemolytic effect, and the hemolysis of MSNs, Ca-Mg@MSNs, DOX@MSNs, and Ca-Mg@DOX@MSNs was less than 5%, which proved that MSNs could be used as a carrier for medical purposes. It could also reduce the hemolysis of DOX. It provides an experimental basis for its further application (Figure 4).

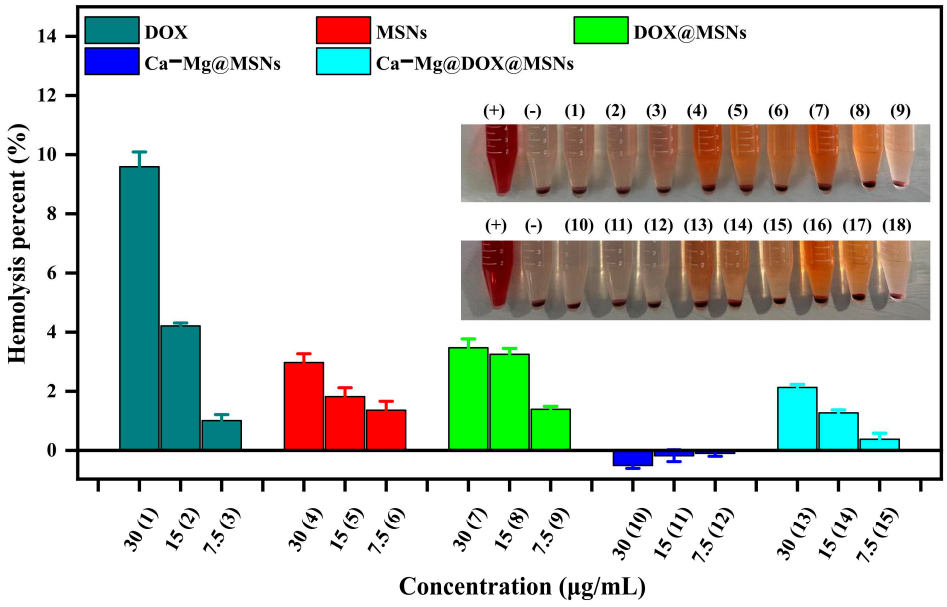

Figure 4. Safety evaluation of Ca-Mg@DOX@MSNs.

2.5. Uptake and In Vitro Anti-Tumor Activity of Ca-Mg@DOX@MSNs

2.5.1. Cellular Uptake of Ca-Mg@DOX@MSNs

FCM measured the uptake of DOX@MSNs and Ca-Mg@DOX@MSNs by 4T1 cells. The uptake of DOX@MSNs and Ca-Mg@DOX@MSNs by 4T1 cells was significantly increased when compared with free DOX, indicating that the prepared nanoparticles can be taken up well by the tumor cells, thus exerting an excellent anti-tumor effect. The prolonged incubation time did not significantly enhance the uptake effect, indicating that the 4T1 cells were able to uptake the DOX@MSNs and Ca-Mg@DOX@MSNs well within a short period (Figure 5a). This result further demonstrates that the prepared DOX@MSNs and Ca-Mg@DOX@MSNs can accumulate in the tumor cells and thus kill the tumor cells to exert excellent anti-tumor effects.

2.5.2. Cellular Toxicity of Ca-Mg@DOX@MSNs

DOX is currently a commonly used drug in breast cancer treatment in clinical practice. As DOX can quickly enter the tumor cells through the cell membranes and act on DNA, it has anti-tumor solid pharmacological activity. As a broad-spectrum anti-tumor drug, it has an inhibitory effect on various tumor cells. However, while killing tumor cells, DOX also produces toxic side effects such as myelosuppression, cardiotoxicity, and liver and kidney functions, which severely limits the clinical application of the drug [41]. Loading DOX with nanocarriers can avoid these drawbacks; to explore this role of the prepared nanocarriers, the toxicity of DOX@MSNs and Ca-Mg@DOX@MSNs on 4T1 cells was determined by the CCK-8 method in this paper. The results at both 24 h and 48 h showed that, with the increasing concentration of the administered drug, the toxicity of DOX, DOX@MSNs, and Ca-Mg @DOX@MSNs significantly enhanced the killing ability of 4T1 cells. Still, the toxicity of DOX@MSNs and Ca-Mg@DOX@MSNs was slightly weaker than that of DOX, which may be attributed to the fact that calcium and magnesium, as trace elements, have the effect of reducing the toxicity of DOX and the property of slightly mitigating the toxicity of DOX, which makes the prepared DOX@MSNs and Ca-Mg@DOX@MSNs reduce the chemotherapeutic toxicity of DOX while exerting anti-tumor effects (Figure 5b).

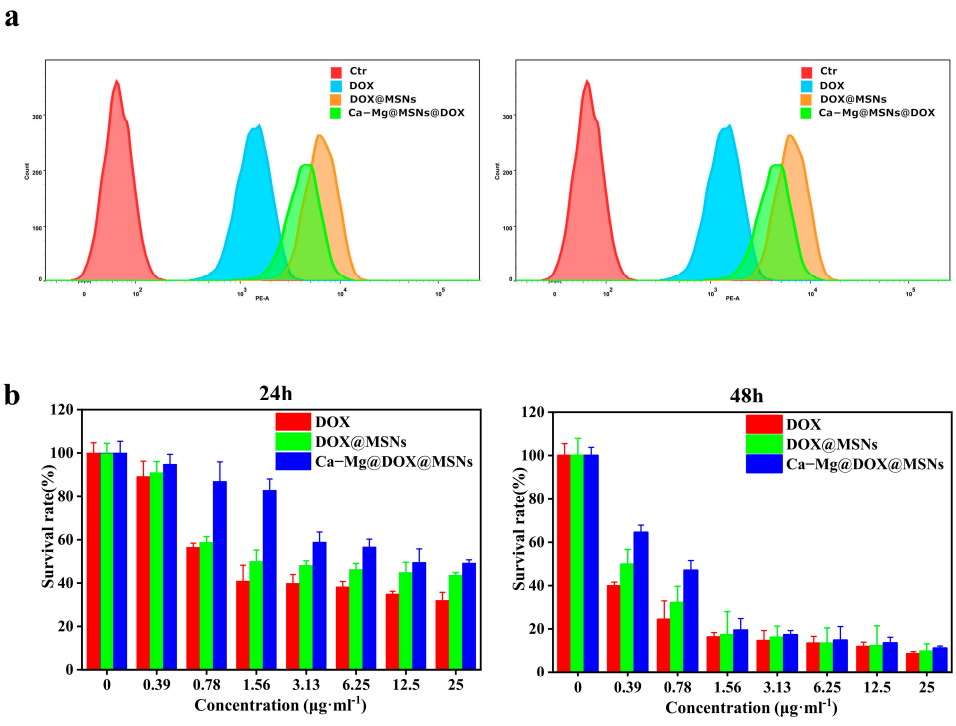

Figure 5. *Cont.*

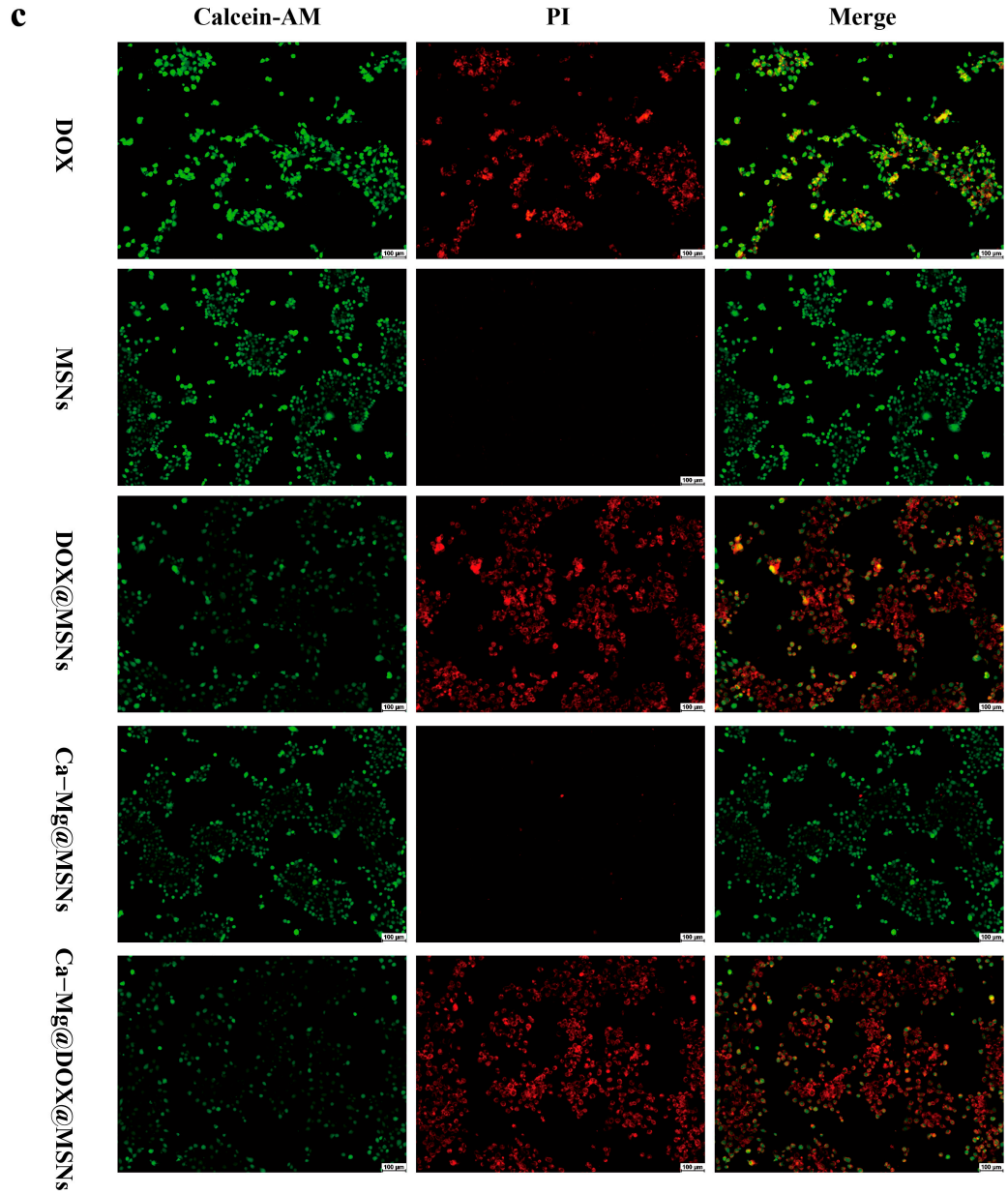

Figure 5. Uptake and in vitro anti-tumor activity of Ca-Mg@DOX@MSNs: (**a**) Results of uptake experiments. (**b**) CCK-8 assay to determine the effects on 4T1 cells. (**c**) Results of live and dead cell staining.

2.5.3. Living/Dead Cell Staining of Ca-Mg@DOX@MSNs

The effects of DOX@MSNs and Ca-Mg@DOX@MSNs on 4T1 cells were observed by the laser confocal staining of live and dead cells. Calcein-AM can pass through the intact cell membrane and embed in the nuclei of all cells (live and dead), showing green fluorescence. PI can only pass through the incomplete cell membrane of the dead cells and be embedded in the nuclei of all dead cells. The nuclei of all dead cells show red fluorescence. From the experimental results, we can see that the red fluorescence in the nuclei of 4T1 cells after the action of DOX@MSNs and Ca-Mg@DOX@MSNs was significantly higher than that of MSNs and Ca-Mg@MSN groups, which indicated that the dead cells were increased by loading DOX. The results were in agreement with the results of CCK-8 (Figure 5c).

3. Discussion

As an emerging nanocarrier, the MSN has potential applications in tumor-targeted drug delivery systems [42–47]. However, the poor biodegradability of MSNs severely hinders its practical biological applications [48,49]. The biodegradation process of conventional MSNs takes days [50] and weeks for excretion from the body [51]. Many studies have shown that poor biodegradability can lead to severe particle bioaccumulation, which may cause [52,53] a range of biosafety issues. Therefore, improving the biodegradability of MSNs is crucial to facilitate their in vivo studies and clinical applications.

Metal ion doping has been reported as an effective strategy to promote MSN biodegradation in the tumor microenvironment. Doping metal ions, such as Mn and Fe, into the silica skeleton to form Si-O-M (M = Mn, Fe, etc.) significantly improved the biodegradability because the M-O bond is more fragile than the Si-O bond in an acidic environment [54]. However, large amounts of Mn, Fe, etc., can harm the human body. Calcium, an essential nutrient element, is commonly used to improve the biodegradability of MSNs compared to other metallic elements by doping into a silica matrix without toxicity. Zhang et al. [55] synthesized MSN/HAP hybrid nanoparticles with good acid-responsive properties by adding calcium salts ($CaCl_2$) and $Na_2HPO_4 \cdot 12\ H_2O$ to the reaction system to make them biodegradable. Similarly, Hu et al. [56] successfully prepared mesoporous silica-calcium phosphate (MS-CAP) hybrid nanoparticles by employing $CaCl_2$ as a Ca^{2+} source, which reacts more readily with Si-OH to form Si-O-Ca than elemental Si. In addition, by TEM observation and ICP-OES analysis, we found that the MS-CAP particles have good stability in neutral and weakly acidic environments (pH 7.4 and pH 6.5). However, in a strongly acidic environment (pH 4.5), the MS-CAP particles were almost completely degraded within 24 h. The MS-CAP particles were also stable in the neutral and weakly acidic environment (pH 7.4 and pH 6.5). In addition, as an essential element, Mg has been used to enhance the biodegradability of MSNs. Yu et al. [40] prepared a pH-responsive biodegradable Mg-doped MSN by the dissolution–re-growth method, in which Mg^{2+}could replace some of the Si in the Si-O-Si to form Mg-O-Si. The Mg-O bond obtained was acid-responsive to fracture, which helped to accelerate the silica particles for biodegradation.

However, most MSNs are doped with only one substance and usually need to exhibit satisfactory biodegradation efficiency. Therefore, multi-substance-doped mesoporous silica with better biodegradability is essential. In this paper, we simultaneously doped two substances, Ca and Mg, into the MSN. The cumulative release of Ca-Mg@DOX@MSNs for 48 h was as high as 92.73 $\pm$ 0.76%, which demonstrated that the simultaneous doping of Ca and Mg could significantly enhance the biodegradability of MSNs and thus could exert an excellent anti-tumor effect. The mechanism may be that pure silica materials are composed of tetrahedra with bridging oxygens with a stable Si-O-Si network structure. For Ca- and Mg-doped mesoporous silica, the presence of Ca and Mg in the silica network structure introduces non-bridging oxygen, resulting in relatively weak Si-O-M (M = Ca, Mg) connections. Therefore, the presence of non-bridging oxygen MS-Ca and MS-Mg in the silica network accelerates the hydrolysis of silica. In addition, the amorphous structure formed by Ca and Mg doping is also believed to favor its degradation [55,57].

Meanwhile, from the cytotoxicity experiments, it can be seen that the doping of Ca and Mg as trace elements into MSNs makes the nanoparticles show the utility of reducing DOX toxicity while killing the tumor cells. This result indicates that the prepared nanoparticles are expected to reduce the toxic side effects of DOX and provide a new idea for the further application of DOX, a broad-spectrum anti-tumor drug, in the clinic.

In summary, the prepared Ca-Mg double-doped MSNs not only significantly enhanced the biodegradation rate of MSNs under acidic conditions, providing a feasible solution to the drawbacks of MSNs in clinical applications at this stage but also showed, due to

Ca-Mg doping of the essential human element, a reduction in DOX toxicity. This surprising discovery provides a basis for the in-depth study of DOX in the clinic, which is expected to be a new strategy for tumor therapy.

4. Materials and Methods

4.1. Materials

The following materials were used: adriamycin hydrochloride (Shanghai McLean Biochemical Technology Co., Ltd., Shanghai, China); tetraethyl silicate-TEOS (Shanghai McLean Biochemical Technology Co., Ltd.); anhydrous ethanol (Tianjin Zhiyuan Chemical Reagent Co., Ltd., Tianjin, China); calcium chloride (Tianjin Xinbute Chemical Co., Ltd., Tianjin, China); magnesium chloride (Tianjin Zhiyuan Chemical Reagent Co., Ltd.); CCK8 (Omer Biotechnology (Shanghai) Co., Ltd., Shanghai, China); live dead cell staining kit (Beijing Solebo Technology Co., Ltd., Beijing, China); and 4T1 cells (Procell Life Science & Technology Co., Ltd, Wuhan, China).

4.2. Preparation of MSNs and Ca-Mg@MSNs

4.2.1. MSNs

After mixing 20 mL of concentrated ammonia and 200 mL of ethanol and heating the water bath to a temperature of 35 °C, 10 mL of TEOS and 100 mL of ethanol were mixed well, and 3/4 of the TEOS ethanol solution was added dropwise to the ammonia–ethanol mixture. The mixture was stirred vigorously in a magnetic stirrer (85-2 temperature-controlled magnetic stirrer, Jintan Medical Instrument Factory) for 30 min; the remaining 1/4 of the TEOS solution was added dropwise, and the reaction was carried out at a temperature of 60 °C for 2 h. After cooling the system to room temperature, it was left to age for 3 h. The mixture was poured into a treated dialysis bag with a cut-off relative molecular mass of 8000~14,000 kDa, and the bag was submerged. The dialysis bag was immersed in deionized water for 3 d, changing the water every 6 h. After dialysis, the bag was freeze-dried and stored at −20 °C [58,59].

4.2.2. Ca-Mg@MSNs

After mixing 20 mL of concentrated ammonia and 200 mL of ethanol and heating the water bath to a temperature of 35 °C, a certain amount of $CaCl_2$ and $MgCl_2$ (specifically, the dosage forms were prepared under Ca^{2+}:Mg^{2+} = 1:1 conditions with 1.25%, 2.5%, and 5% $CaCl_2$ and $MgCl_2$ concentration gradients, respectively), 10 mL of TEOS, and 100 mL of ethanol were mixed homogeneously, and 3/4 of the TEOS ethanol solution was taken and added dropwise to the ammonia–ethanol mixed solution. Stir vigorously for 30 min; add the remaining 1/4 of TEOS solution dropwise; and react for 2 h at a temperature of 60 °C. After the system was cooled down to room temperature and left to age for 3 h, the mixture was poured into a treated dialysis bag with a cut-off relative molecular mass of 8000–14,000 kDa. The bag was submerged in deionized water for dialysis for 3 d. During this period, the water was changed every 6 h, and, after the end of dialysis, the resulting samples were freeze-dried and stored at −20 °C [55].

4.3. Characterization of MSNs and Ca-Mg@MSNs

4.3.1. Particle Size, Potential, and Morphology

A certain amount of MSNs and Ca-Mg@MSNs was taken in a specific volume of deionized water. Ultrasonic oscillation (KQ5200DE, CNC ultrasonic cleaner, Jiangsu, China) was used to disperse the nanoparticles nicely. The particle size was determined by using a laser particle size analyzer (Nano-2S90, Malvern Laser Particle Sizing, Malvern, UK), and the potential and PDI were determined using a laser particle size analyzer (Nano-2S90,

Malvern Laser Particle Sizing, Malvern, UK) [60]. After coating the MSNs at an accelerating voltage of 5.0 kV, their morphology and dimensions were analyzed by scanning electron microscopy [57].

4.3.2. EDX Mapping Analysis

A certain amount of Ca-Mg@MSNs was placed on the scanning electron microscope (JSM-7610FPlus, thermal field emission scanning electron microscope, Tokyo, Japan), and nanoparticles were irradiated by X-rays. The element's intra-atomic shell electrons were excited, produced shell electron leaps, and emitted the element's characteristics of X-rays. Through the detector to measure the wavelength of the characteristic X-rays of the element (energy) of the intensity of the concentration of the ratio of the relationship between the wavelength of the X-rays, it will be able to carry out a quantitative analysis of the wavelength dispersive X-ray fluorescence spectrometry.

4.4. Preparation of DOX@MSNs and Ca-Mg@DOX@MSNs

The DOX was adsorbed on the surfaces of MSNs and Ca-Mg@MSNs by non-covalent bonding. MSNs and Ca-Mg@MSNs were dispersed in the DOX aqueous solution with concentrations of 250, 500, and 750 ug/mL, respectively, and, after standing for 30 min, the probes were ultrasonicated for 5 min, which led to the preparation of DOX@MSNs and Ca-Mg@DOX@MSNs [61].

4.5. Characterization of DOX@MSNs and Ca-Mg@DOX@MSNs

4.5.1. Specific Surface Area and Pore Size Analysis (BET)

N_2 adsorption–desorption isotherms were carried out on a Micromeritics ASAP2460 analyzer (ASAP 2460, Micromeritics Instrument Corporation, Norfolk, USA) at 77.3 K under continuous adsorption conditions. The samples were processed under vacuum at 200 °C for 4 h prior to nitrogen adsorption. The specific surface area was calculated from the adsorption and desorption isotherms of the samples according to the BET formula, and the pore size distribution was calculated using the BJH equivalent cylindrical model.

4.5.2. Particle Size, Potential, Morphology, Loading, and Encapsulation Efficiency of DOX@MSNs and Ca-Mg@DOX@MSNs

A certain amount of DOX@MSNs and Ca-Mg@DOX@MSNs were taken in a specific volume of deionized water. Ultrasonic oscillation was used to make the nanoparticles fully dispersed, and a laser particle size analyzer was used to determine the particle size, potential, and PDI [62]. After coating the MSNs at an accelerating voltage of 5.0 kV, their morphology and dimensions were analyzed by scanning electron microscopy.

Take a certain amount of the ultrafiltered off DOX small molecule solution, measure the absorbance with the UV2550 UV–visible spectrophotometer (Shanghai Optical Instrument Factory Co., Ltd., Shanghai, China), calculate the drug concentration by substituting into the standard curve equation, and calculate the encapsulation efficiency according to Equation (1). Weigh the same volume of DOX@MSNs and Ca-Mg@DOX@MSNs, freeze dry, and then calculate the drug loading efficiency according to Equation (2):

$$\text{Encapsulationefficiency}(\%) = \frac{\begin{array}{c}\text{Amountofdrugina definite}\\ \text{massofthepreparedparticle (mg)}\end{array}}{\begin{array}{c}\text{Theoreticalamountof}\\ \text{druginthesamemass (mg)}\end{array}} \times 100\% \quad (1)$$

$$\text{Loadingefficiency}(\%) = \frac{\text{Amountofdrugina definite massofthepreparedparticle (mg)}}{\text{Totalmassoftheparticles (mg)}} \times 100\% \quad (2)$$

4.6. Release of Ca-Mg@DOX@MSNs

4.6.1. Calculated Results of Molecular Dynamic Simulations of Ca-Mg@DOX@MSNs

We have employed molecular dynamic computer simulations to investigate the structure and properties of Ca-Mg-doped MSNs. All calculations were carried out using the pseudopotential plane wave method based on first principles, performed by the CASTEP software package (V23.1.1) [63], and their surface charges were calculated using density-functional theory (DFT) [64].

4.6.2. Cumulative Release of Ca-Mg@DOX@MSNs

A total of 2 mL of DOX@MSNs, Ca-Mg@DOX@MSNs, and the DOX solution (the amount of DOX was 250 ug/mL) were taken in a dialysis bag (molecular weight cut-off 3500), clamped at both ends, and then placed in the dissolution medium containing 200 mL of isotonic PBS. The temperature was kept at (37 ± 0.5) °C, and the rate was 500 r/min (ZWYR-D2402 Zhicheng constant temperature culture oscillator, Shanghai Zhicheng Analytical Instrument Manufacturing Co., Shanghai, China). Samples of 2 mL were taken at 10 min, 20 min, 30 min, 1.0 h, 2.0 h, 3.0 h, 4.0 h, 6.0 h, 8.0 h, 24 h, and 48 h (immediately supplemented with isotonic PBS at the same temperature and same volume). The drug concentration was determined using a UV–visible spectrophotometer at 488 nm, and the cumulative release rate was calculated and fitted to cumulative releases and time. The test was repeated three times to obtain the mean value [65,66].

4.7. Safety Evaluation of Ca-Mg@DOX@MSNs

Hemolysis Experiment of Ca-Mg@DOX@MSNs

Using saline as the negative control and distilled water as the positive control, dilute 10 mL each of MSNs, DOX@MSNs, Ca-Mg@MSNs, Ca-Mg@DOX@MSNs, and DOX (DOX concentrations of 30 μg/mL, 15 μg/mL, and 7.5 μg/mL) with saline and incubate for 30 min in a 37 °C water bath, adding freshly diluted anticoagulated blood of 0.2 mL, mixing them evenly. After homogenization, incubate at 37 °C for 60 min, centrifuge at 3000 r/min for 10 min, take the supernatant, and measure the OD value at 545 nm, three times in parallel, for the evaluation of hemolysis efficiency according to Equation (3).

$$\text{Hemolysisefficiency}(\%) = \frac{\text{OD}_{\text{Sample}} - \text{OD}_{\text{Negative}}}{\text{OD}_{\text{Positive}} - \text{OD}_{\text{Negative}}} \times 100\% \quad (3)$$

The OD value of the negative control group is less than 0.03, and that of the positive control group is 0.8 ± 0.3. If the hemolysis efficiency of the material is less than 5%, it conforms to the requirements of the hemolysis experiment of medical materials; if the hemolysis efficiency is more than 5%, it fails to conform to the requirements.

4.8. Uptake and In Vitro Anti-Tumor Activity of Ca-Mg@DOX@MSNs

4.8.1. Cellular Uptake of Ca-Mg@DOX@MSNs

4T1 cells were inoculated into six-well plates (5×10^5/well) and incubated overnight at 37 °C, 5% CO_2, and suitable humidity. DOX, DOX@MSNs, and Ca-Mg@DOX@MSNs (DOX content 1 ug/mL) were added, respectively, along with a blank control, and, after 2 h and 24 h of action, the cells were washed three times with PBS, digested, centrifuged at 1000 r/min, and resuspended with PBS. Sieving was performed, flow cytometry (LSR-II, BD, USA) was performed, and FlowJo analyzed the data [67].

4.8.2. Cellular Toxicity of Ca-Mg@DOX@MSNs

4T1 cells were cultured in DMEM medium with 10% FBS and 1% antibiotics (100 U/mL of penicillin and 100 μg/mL of streptomycin). After the cells grow to the logarithmic growth phase, inoculate into 96-well culture plates (5000/well) and incubate overnight at 37 °C, 5% CO_2, and suitable humidity. After adding DOX@MSNs and Ca-Mg@DOX@MSNs (DOX concentrations of 0, 3.12, 5.25, 12.50, 25.00, and 50.00 μg/mL), respectively, along with a blank control and negative control, with five replicate wells in each group, and after 24 h and 48 h of action, add 20 μL of the CCK-8 solution (5 mg/mL) and incubate for 2 h. Absorbance was measured at 450 nm by an enzyme labeling instrument (Multiskan FC, Enzyme-Linked Immunosorbent Assay Analyzer, Waltham, US.), and the cell survival rate was calculated according to Equation (4) [68]:

$$\text{Cellsurvivalrate}(\%) = \frac{\text{Experimentalgroup} - \text{Blankcontrol}}{\text{Negativecontrol} - \text{Blankcontrol}} \times 100\% \quad (4)$$

4.8.3. Living/Dead Cell Staining of Ca-Mg@DOX@MSNs

The 4T1 cells were inoculated onto confocal culture dishes (5000/well) and incubated overnight at 37 °C, 5% CO_2, and suitable humidity. DOX@MSNs and Ca-Mg@DOX@MSNs (DOX concentration of 1 μg/mL) were added. At the same time, a blank control was set up, and, after 24 h of action, the cells were washed three times with PBS and added 100 μL of a 2 μM Calcein-AM working solution and a 4.5 μM PI working solution to each well. The cells were incubated for 30 min, and the cells were washed three times with PBS. The 100 μL PBS in LSCM (Nanjing Henqiao Instrument Co., Ltd., Nanjing, China) observed cell status [69].

5. Conclusions

In this study, Ca-Mg-doped MSNs were prepared, significantly increasing their biodegradation rate because Ca-O and Mg-O bonds are more fragile than Si-O bonds in an acidic environment. The MSNs and DOX@MSNs were successfully synthesized with a particle size of approximately 200–300 nm and exhibited a negative charge. Both MSNs and DOX@MSNs exhibited a regular spherical morphology, whereas the Ca and Mg-doped nanoparticles displayed an irregular spherical shape. Elemental mapping revealed that the Ca and Mg contents were 2.92% and 1.19%, respectively. The DOX@MSNs and Ca-Mg@DOX@MSNs were also successfully prepared, with a particle size ranging from 300 to 400 nm and a negative charge. The encapsulation efficiency was approximately 90%, and the drug loading efficiency was around 10%. Notably, these nanoparticles demonstrated a slower drug release compared to free DOX in solution. The release of Ca-Mg@DOX@MSNs was notably accelerated under acidic conditions. All samples exhibited a hemolysis rate of less than 5%. Cellular toxicity assays revealed that DOX@MSNs and Ca-Mg@DOX@MSNs exhibited lower toxicity compared to free DOX. Similar results were observed in live/dead cell staining experiments. Furthermore, cellular uptake studies indicated that DOX@MSNs were taken up more efficiently than Ca-Mg@DOX@MSNs and free DOX. In conclusion, this study provides new insights into the treatment of breast cancer by selecting essential and non-toxic elements to optimize the properties of MSN materials, which significantly increased drug release and reduced chemotherapeutic drug toxicity.

It is important to acknowledge that, while this study offers promising insights into breast cancer treatment, there are several limitations that require further attention in future research. First, although this study highlights that DOX@MSNs and Ca-Mg@DOX@MSNs can effectively reduce the toxicity of DOX and exhibit anti-tumor effects, the experiments were primarily conducted in vitro using 4T1 cell lines. This study did not include other

tumor cell lines or clinical samples, which limits the broader applicability of these findings. Tumor types and individual patient variability may result in differences in the performance of these materials. Therefore, expanding research to include various tumor models and preclinical animal experiments is crucial to better assess the clinical translational potential of these materials. Moreover, the preparation method for calcium and magnesium-doped MSN materials used in this study has not been validated in vivo. While the method has shown some success in vitro, its reproducibility and scalability have not been fully confirmed. Although relevant preparation techniques are available in the literature, industrial-scale applications may face challenges such as high production costs and potential material instability. Hence, future research should focus on developing methods for controllable synthesis, large-scale production, cost reduction, and ensuring the long-term stability of these materials.

Author Contributions: Conceptualization, Q.Z., X.T. and M.W.; methodology, Q.Z., X.T. and M.W.; investigation, Q.Z., J.H., R.C., T.J., Y.H., T.B. and X.T.; resources, M.W.; data curation, Q.Z., X.T. and M.W.; writing—original draft preparation, Q.Z., C.L. and X.T.; writing—review and editing, Q.Z., C.L., X.T. and M.W.; formal analysis, J.H., R.C., Y.H., T.B. and T.J.; supervision, C.L. and M.W.; project administration, C.L. and M.W.; funding acquisition, C.L. and M.W. All authors have read and agreed to the published version of the manuscript.

Funding: This study was funded by the National Science Foundation of China (No. 82460366), the Particular Project of Innovation Environment Construction in Autonomous Region of Xinjiang-Construction of Science and Technology Innovation Base (PT2304), the Special Funds for Xinjiang Key Laboratory of Natural Medicines Active Components and Drug Release Technology, Engineering Research Center of Xinjiang and Central Asian Medicine Resources, Ministry of Education.

Data Availability Statement: Data is contained within the article.

Conflicts of Interest: The authors have no financial or proprietary interests in any material discussed in this article.

References

1. Sung, H.; Ferlay, J.; Siegel, R.L.; Laversanne, M.; Soerjomataram, I.; Jemal, A.; Bray, F. Global Cancer Statistics 2020: GLOBOCAN Estimates of Incidence and Mortality Worldwide for 36 Cancers in 185 Countries. *CA Cancer J. Clin.* **2021**, *71*, 209–249. [CrossRef] [PubMed]
2. Cainap, C.; Crisan, N. Advances in Cancer Therapy from Research to Clinical Practice—Surgical, Molecular or Systemic Management of Cancer. *Medicina* **2023**, *59*, 1309. [CrossRef] [PubMed]
3. Qi, J.; Li, M.; Wang, L.; Hu, Y.; Liu, W.; Long, Z.; Zhou, Z.; Yin, P.; Zhou, M. National and Subnational Trends in Cancer Burden in China, 2005-20: An Analysis of National Mortality Surveillance Data. *Lancet Public Health* **2023**, *8*, e943–e955. [CrossRef] [PubMed]
4. Bray, F.; Ferlay, J.; Soerjomataram, I.; Siegel, R.L.; Torre, L.A.; Jemal, A. Global Cancer Statistics 2018: GLOBOCAN Estimates of Incidence and Mortality Worldwide for 36 Cancers in 185 Countries. *CA Cancer J. Clin.* **2018**, *68*, 394–424. [CrossRef] [PubMed]
5. Wang, J.; Wu, S.-G. Breast Cancer: An Overview of Current Therapeutic Strategies, Challenge, and Perspectives. *Breast Cancer Targets Ther.* **2023**, *15*, 721–730. [CrossRef]
6. Debien, V.; De Caluwé, A.; Wang, X.; Piccart-Gebhart, M.; Tuohy, V.K.; Romano, E.; Buisseret, L. Immunotherapy in Breast Cancer: An Overview of Current Strategies and Perspectives. *NPJ Breast Cancer* **2023**, *9*, 7. [CrossRef] [PubMed]
7. Zarenezhad, E.; Kanaan, M.H.G.; Abdollah, S.S.; Vakil, M.K.; Marzi, M.; Mazarzaei, A.; Ghasemian, A. Metallic Nanoparticles: Their Potential Role in Breast Cancer Immunotherapy via Trained Immunity Provocation. *Biomedicines* **2023**, *11*, 1245. [CrossRef] [PubMed]
8. Yu, L.-Y.; Tang, J.; Zhang, C.-M.; Zeng, W.-J.; Yan, H.; Li, M.-P.; Chen, X.-P. New Immunotherapy Strategies in Breast Cancer. *Int. J. Environ. Res. Public Health* **2017**, *14*, 68. [CrossRef]
9. Zhang, R.; Clark, S.D.; Guo, B.; Zhang, T.; Jeansonne, D.; Jeyaseelan, S.J.; Francis, J.; Huang, W. Challenges in the Combination of Radiotherapy and Immunotherapy for Breast Cancer. *Expert Rev. Anticancer Ther.* **2023**, *23*, 375–383. [CrossRef]
10. Du, Y. Research Progress of Tumor Microenvironment-Responsive Anti-Tumor Nano-Drug Carriers. *BIO Web Conf.* **2023**, *61*, 01031. [CrossRef]

11. Pal, S.; Mehta, D.; Dasgupta, U.; Bajaj, A. Advances in Engineering of Low Molecular Weight Hydrogels for Chemotherapeutic Applications. *Biomed. Mater. Bristol Engl.* **2021**, *16*, 024102. [CrossRef] [PubMed]
12. Maksymowicz, M.; Machowiec, P.; Korzeniowska, A.; Baran, N.; Bielak, A.; Nowak, A.; Cywka, Ł.; Szwed, W.; Nowak, A.; Bogusz, K. Adverse Effects in the Management of Breast Cancer—Recent Studies. *J. Educ. Health Sport* **2023**, *37*, 11–24. [CrossRef]
13. Li, L.; Yang, W.-W.; Xu, D.-G. Stimuli-Responsive Nanoscale Drug Delivery Systems for Cancer Therapy. *J. Drug Target.* **2019**, *27*, 423–433. [CrossRef] [PubMed]
14. Xiang, J.; Zhao, R.; Wang, B.; Sun, X.; Guo, X.; Tan, S.; Liu, W. Advanced Nano-Carriers for Anti-Tumor Drug Loading. *Front. Oncol.* **2021**, *11*, 758143. [CrossRef] [PubMed]
15. Ta, Q.T.H. Highly Surface-Active Si-Doped TiO_2/$Ti_3C_2T_x$ Heterostructure for Gas Sensing and Photodegradation of Toxic Matters. *Chem. Eng. J.* **2021**, *425*, 131437. [CrossRef]
16. Tran, M.N.; Moreau, M.; Addad, A.; Teurtrie, A.; Roland, T.; de Waele, V.; Dewitte, M.; Thomas, L.; Levêque, G.; Dong, C.; et al. Boosting Gas-Phase TiO_2 Photocatalysis with Weak Electric Field Strengths of Volt/Centimeter. *ACS Appl. Mater. Interfaces* **2024**, *16*, 14852–14863. [CrossRef]
17. Deng, S.; Cui, C.-X.; Duan, L.; Hu, L.; Yang, X.; Wang, J.-C.; Qu, L.-B.; Zhang, Y. Anticancer Drug Release System Based on Hollow Silica Nanocarriers Triggered by Tumor Cellular Microenvironments. *ACS Omega* **2021**, *6*, 553–558. [CrossRef] [PubMed]
18. Yang, W.; Yang, S.; Jiang, L.; Zhou, Y.; Yang, C.; Deng, C. Tumor Microenvironment Triggered Biodegradation of Inorganic Nanoparticles for Enhanced Tumor Theranostics. *RSC Adv.* **2020**, *10*, 26742–26751. [CrossRef] [PubMed]
19. Chiou, A.E.; Hinckley, J.A.; Khaitan, R.; Varsano, N.; Wang, J.; Malarkey, H.F.; Hernandez, C.J.; Williams, R.M.; Estroff, L.A.; Weiner, S.; et al. Fluorescent Silica Nanoparticles to Label Metastatic Tumor Cells in Mineralized Bone Microenvironments. *Small* **2021**, *17*, e2001432. [CrossRef]
20. Zhao, H.; Li, Y.; Chen, J.; Zhang, J.; Yang, Q.; Cui, J.; Shi, A.; Wu, J. Environmental Stimulus-Responsive Mesoporous Silica Nanoparticles as Anticancer Drug Delivery Platforms. *Colloids Surf. B Biointerfaces* **2024**, *234*, 113758. [CrossRef]
21. Hosseinpour, S.; Walsh, L.J.; Xu, C. Biomedical Application of Mesoporous Silica Nanoparticles as Delivery Systems: A Biological Safety Perspective. *J. Mater. Chem. B* **2020**, *8*, 9863–9876. [CrossRef]
22. Croissant, J.G.; Fatieiev, Y.; Khashab, N.M. Degradability and Clearance of Silicon, Organosilica, Silsesquioxane, Silica Mixed Oxide, and Mesoporous Silica Nanoparticles. *Adv. Mater.* **2017**, *29*, 1604634. [CrossRef] [PubMed]
23. Niculescu, V.-C. Mesoporous Silica Nanoparticles for Bio-Applications. *Front. Mater.* **2020**, *7*, 36. [CrossRef]
24. Manzano, M.; Vallet-Regí, M. Mesoporous Silica Nanoparticles in Nanomedicine Applications. *J. Mater. Sci. Mater. Med.* **2018**, *29*, 65. [CrossRef] [PubMed]
25. Yue, J.; Luo, S.-Z.; Lu, M.-M.; Shao, D.; Wang, Z.; Dong, W.-F. A Comparison of Mesoporous Silica Nanoparticles and Mesoporous Organosilica Nanoparticles as Drug Vehicles for Cancer Therapy. *Chem. Biol. Drug Des.* **2018**, *92*, 1435–1444. [CrossRef] [PubMed]
26. Zhang, W.; Liu, H.; Qiu, X.; Zuo, F.; Wang, B. Mesoporous Silica Nanoparticles as a Drug Delivery Mechanism. *Open Life Sci.* **2024**, *19*, 20220867. [CrossRef] [PubMed]
27. Zhou, J.; Liu, C.; Zhong, Y.; Luo, Z.; Wu, L. A Review of Current Developments in Functionalized Mesoporous Silica Nanoparticles: From Synthesis to Biosensing Applications. *Biosensors* **2024**, *14*, 575. [CrossRef]
28. Kovtareva, S.; Kusepova, L.; Tazhkenova, G.; Mashan, T.; Bazarbaeva, K.; Kopishev, E. Surface Modification of Mesoporous Silica Nanoparticles for Application in Targeted Delivery Systems of Antitumour Drugs. *Polymers* **2024**, *16*, 1105. [CrossRef]
29. Pohaku Mitchell, K.K.; Liberman, A.; Kummel, A.C.; Trogler, W.C. Iron(III)-Doped, Silica Nanoshells: A Biodegradable Form of Silica. *J. Am. Chem. Soc.* **2012**, *134*, 13997–14003. [CrossRef] [PubMed]
30. Alexis, F.; Pridgen, E.; Molnar, L.K.; Farokhzad, O.C. Factors Affecting the Clearance and Biodistribution of Polymeric Nanoparticles. *Mol. Pharm.* **2008**, *5*, 505–515. [CrossRef]
31. Patwardhan, S.V.; Emami, F.S.; Berry, R.J.; Jones, S.E.; Naik, R.R.; Deschaume, O.; Heinz, H.; Perry, C.C. Chemistry of Aqueous Silica Nanoparticle Surfaces and the Mechanism of Selective Peptide Adsorption. *J. Am. Chem. Soc.* **2012**, *134*, 6244–6256. [CrossRef] [PubMed]
32. Dechézelles, J.-F.; Ciotonea, C.; Catrinescu, C.; Ungureanu, A.; Royer, S.; Nardello-Rataj, V. Emulsions Stabilized with Alumina-Functionalized Mesoporous Silica Particles. *Langmuir ACS J. Surf. Colloids* **2020**, *36*, 3212–3220. [CrossRef]
33. Hu, Y.; Bai, S.; Wu, X.; Tan, S.; He, Y. Biodegradability of Mesoporous Silica Nanoparticles. *Ceram. Int.* **2021**, *47*, 31031–31041. [CrossRef]
34. Liu, C.-G.; Han, Y.-H.; Zhang, J.-T.; Kankala, R.K.; Wang, S.-B.; Chen, A.-Z. Rerouting Engineered Metal-Dependent Shapes of Mesoporous Silica Nanocontainers to Biodegradable Janus-Type (Sphero-Ellipsoid) Nanoreactors for Chemodynamic Therapy. *Chem. Eng. J.* **2019**, *370*, 1188–1199. [CrossRef]
35. Zhang, Y.; Lin, X.; Chen, X.; Fang, W.; Yu, K.; Gu, W.; Wei, Y.; Zheng, H.; Piao, J.; Li, F. Strategies to Regulate the Degradation and Clearance of Mesoporous Silica Nanoparticles: A Review. *Int. J. Nanomed.* **2024**, *19*, 5859–5878. [CrossRef]
36. Liu, C.; Tang, X.; Huang, G. Biodegradable Ca^{2+} Doped Mesoporous Silica Nanoparticles Promote Chemotherapy Synergism with Calcicoptosis and Activate Anti-Tumor Immunity. *Inorganics* **2024**, *12*, 152. [CrossRef]

37. Sarkar, R.; Biswas, S.; Ghosh, R.; Samanta, P.; Pakhira, S.; Mondal, M.; Dutta Gupta, Y.; Bhandary, S.; Saha, P.; Bhowmik, A.; et al. Exosome-Sheathed Porous Silica Nanoparticle-Mediated Co-Delivery of 3,3′-Diindolylmethane and Doxorubicin Attenuates Cancer Stem Cell-Driven EMT in Triple Negative Breast Cancer. *J. Nanobiotechnol.* **2024**, *22*, 285. [CrossRef]
38. Tang, L.; Chen, M.; Wang, D.; He, Y.; Ge, G.; Zeng, Z.; Shu, J.; Guo, W.; Wu, S.X.; Xiong, W. Doxorubicin and Iron-Doped Mesoporous Silica Nanoparticles for Chemodynamic Therapy and Chemotherapy of Breast Cancer. *New J. Chem.* **2024**, *48*, 17294–17309. [CrossRef]
39. He, Y.; Shao, L.; Hu, Y.; Zhao, F.; Tan, S.; He, D.; Pan, A. Redox and pH Dual-Responsive Biodegradable Mesoporous Silica Nanoparticle as a Potential Drug Carrier for Synergistic Cancer Therapy. *Ceram. Int.* **2021**, *47*, 4572–4578. [CrossRef]
40. Yu, L.; Chen, Y.; Lin, H.; Gao, S.; Chen, H.; Shi, J. Magnesium-Engineered Silica Framework for pH-Accelerated Biodegradation and DNAzyme-Triggered Chemotherapy. *Small* **2018**, *14*, e1800708. [CrossRef] [PubMed]
41. Wang, Y.; Chen, X.; He, D.; Zhou, Y.; Qin, L. Surface-Modified Nanoerythrocyte Loading DOX for Targeted Liver Cancer Chemotherapy. *Mol. Pharm.* **2018**, *15*, 5728–5740. [CrossRef] [PubMed]
42. Chen, Y.; Ma, H.; Wang, W.; Zhang, M. A Size-Tunable Nanoplatform: Enhanced MMP2-Activated Chemo-Photodynamic Immunotherapy Based on Biodegradable Mesoporous Silica Nanoparticles. *Biomater. Sci.* **2021**, *9*, 917–929. [CrossRef]
43. Esfahani, M.K.M.; Islam, N.; Cabot, P.J.; Izake, E.L. Development of Thiabendazole-Loaded Mesoporous Silica Nanoparticles for Cancer Therapy. *ACS Biomater. Sci. Eng.* **2022**, *8*, 4153–4162. [CrossRef] [PubMed]
44. Cheng, D.; Ji, Y.; Wang, B.; Wang, Y.; Tang, Y.; Fu, Y.; Xu, Y.; Qian, X.; Zhu, W. Dual-Responsive Nanohybrid Based on Degradable Silica-Coated Gold Nanorods for Triple-Combination Therapy for Breast Cancer. *Acta Biomater.* **2021**, *128*, 435–446. [CrossRef] [PubMed]
45. Choi, G.; Rejinold, N.S.; Piao, H.; Choy, J.-H. Inorganic-Inorganic Nanohybrids for Drug Delivery, Imaging and Photo-Therapy: Recent Developments and Future Scope. *Chem. Sci.* **2021**, *12*, 5044–5063. [CrossRef] [PubMed]
46. Lin, F.-C.; Xie, Y.; Deng, T.; Zink, J.I. Magnetism, Ultrasound, and Light-Stimulated Mesoporous Silica Nanocarriers for Theranostics and Beyond. *J. Am. Chem. Soc.* **2021**, *143*, 6025–6036. [CrossRef]
47. Kankala, R.K.; Han, Y.-H.; Na, J.; Lee, C.-H.; Sun, Z.; Wang, S.-B.; Kimura, T.; Ok, Y.S.; Yamauchi, Y.; Chen, A.-Z.; et al. Nanoarchitectured Structure and Surface Biofunctionality of Mesoporous Silica Nanoparticles. *Adv. Mater.* **2020**, *32*, e1907035. [CrossRef]
48. Cheng, Y.; Jiao, X.; Fan, W.; Yang, Z.; Wen, Y.; Chen, X. Controllable Synthesis of Versatile Mesoporous Organosilica Nanoparticles as Precision Cancer Theranostics. *Biomaterials* **2020**, *256*, 120191. [CrossRef]
49. Nguyen, T.L.; Choi, Y.; Kim, J. Mesoporous Silica as a Versatile Platform for Cancer Immunotherapy. *Adv. Mater.* **2019**, *31*, e1803953. [CrossRef] [PubMed]
50. Yamada, H.; Urata, C.; Aoyama, Y.; Osada, S.; Yamauchi, Y.; Kuroda, K. Preparation of Colloidal Mesoporous Silica Nanoparticles with Different Diameters and Their Unique Degradation Behavior in Static Aqueous Systems. *Chem. Mater.* **2012**, *24*, 1462–1471. [CrossRef]
51. Liu, T.; Li, L.; Teng, X.; Huang, X.; Liu, H.; Chen, D.; Ren, J.; He, J.; Tang, F. Single and Repeated Dose Toxicity of Mesoporous Hollow Silica Nanoparticles in Intravenously Exposed Mice. *Biomaterials* **2011**, *32*, 1657–1668. [CrossRef] [PubMed]
52. Yang, G.; Phua, S.Z.F.; Bindra, A.K.; Zhao, Y. Degradability and Clearance of Inorganic Nanoparticles for Biomedical Applications. *Adv. Mater.* **2019**, *31*, e1805730. [CrossRef] [PubMed]
53. Kempen, P.J.; Greasley, S.; Parker, K.A.; Campbell, J.L.; Chang, H.-Y.; Jones, J.R.; Sinclair, R.; Gambhir, S.S.; Jokerst, J.V. Theranostic Mesoporous Silica Nanoparticles Biodegrade after Pro-Survival Drug Delivery and Ultrasound/Magnetic Resonance Imaging of Stem Cells. *Theranostics* **2015**, *5*, 631–642. [CrossRef]
54. Wang, X.; Li, X.; Ito, A.; Sogo, Y.; Watanabe, Y.; Tsuji, N.M.; Ohno, T. Biodegradable Metal Ion-Doped Mesoporous Silica Nanospheres Stimulate Anticancer Th1 Immune Response in Vivo. *ACS Appl. Mater. Interfaces* **2017**, *9*, 43538–43544. [CrossRef]
55. Hao, X.; Hu, X.; Zhang, C.; Chen, S.; Li, Z.; Yang, X.; Liu, H.; Jia, G.; Liu, D.; Ge, K.; et al. Hybrid Mesoporous Silica-Based Drug Carrier Nanostructures with Improved Degradability by Hydroxyapatite. *ACS Nano* **2015**, *9*, 9614–9625. [CrossRef] [PubMed]
56. He, Y.; Zeng, B.; Liang, S.; Long, M.; Xu, H. Synthesis of pH-Responsive Biodegradable Mesoporous Silica-Calcium Phosphate Hybrid Nanoparticles as a High Potential Drug Carrier. *ACS Appl. Mater. Interfaces* **2017**, *9*, 44402–44409. [CrossRef] [PubMed]
57. Wang, X.; Li, X.; Ito, A.; Sogo, Y. Synthesis and Characterization of Hierarchically Macroporous and Mesoporous CaO–MO–SiO_2–P_2O_5 (M = Mg, Zn, Sr) Bioactive Glass Scaffolds. *Acta Biomater.* **2011**, *7*, 3638–3644. [CrossRef] [PubMed]
58. Pan, L.; He, Q.; Liu, J.; Chen, Y.; Ma, M.; Zhang, L.; Shi, J. Nuclear-Targeted Drug Delivery of TAT Peptide-Conjugated Monodisperse Mesoporous Silica Nanoparticles. *J. Am. Chem. Soc.* **2012**, *134*, 5722–5725. [CrossRef] [PubMed]
59. Sarkar, S.; Ekbal Kabir, M.; Kalita, J.; Manna, P. Mesoporous Silica Nanoparticles: Drug Delivery Vehicles for Antidiabetic Molecules. *ChemBioChem* **2023**, *24*, e202200672. [CrossRef]
60. Chen, W.-S.; Chen, H.-R.; Lee, C.-H. The Photocatalytic Performance of Ag-Decorated SiO_2 Nanoparticles (NPs) and Binding Ability between Ag NPs and Modifiers. *Coatings* **2022**, *12*, 146. [CrossRef]

61. Nguyen, T.N.; Nguyen, T.T.; Nghiem, T.H.L.; Nguyen, D.T.; Tran, T.T.H.; Vu, D.; Nguyen, T.B.N.; Nguyen, T.M.H.; Nguyen, V.T.; Nguyen, M.H. Optical Properties of Doxorubicin Hydrochloride Load and Release on Silica Nanoparticle Platform. *Molecules* **2021**, *26*, 3968. [CrossRef] [PubMed]
62. Yang, M.; Yang, W.; Chen, L.; Ding, M.; Li, C.; Shi, D. A Novel Synthesis of Fe_3O_4@SiO_2@Au@Porous SiO_2 Structure for NIR Irradiation-Induced DOX Release and Cancer Treatment. *Dose-Response Publ. Int. Hormesis Soc.* **2020**, *18*, 1559325820906662. [CrossRef]
63. Segall, M.D.; Lindan, P.J.D.; Probert, M.J.; Pickard, C.J.; Hasnip, P.J.; Clark, S.J.; Payne, M.C. First-Principles Simulation: Ideas, Illustrations and the CASTEP Code. *J. Phys. Condens. Matter* **2002**, *14*, 2717–2744. [CrossRef]
64. Grimme, S.; Antony, J.; Ehrlich, S.; Krieg, H. A Consistent and Accurate Ab Initio Parametrization of Density Functional Dispersion Correction (DFT-D) for the 94 Elements H-Pu. *J. Chem. Phys.* **2010**, *132*, 154104. [CrossRef] [PubMed]
65. Cai, W.; Guo, M.; Weng, X.; Zhang, W.; Owens, G.; Chen, Z. Modified Green Synthesis of Fe_3O_4@SiO_2 Nanoparticles for pH Responsive Drug Release. *Mater. Sci. Eng. C Mater. Biol. Appl.* **2020**, *112*, 110900. [CrossRef] [PubMed]
66. Mirzaei-Kalar, Z.; Kiani Nejad, Z.; Khandar, A.A. New $ZnFe_2O_4$@SiO_2@graphene Quantum Dots as an Effective Nanocarrier for Targeted DOX Delivery and CT-DNA Binder. *J. Mol. Liq.* **2022**, *363*, 119904. [CrossRef]
67. Trushina, D.B.; Sapach, A.Y.; Burachevskaia, O.A.; Medvedev, P.V.; Khmelenin, D.N.; Borodina, T.N.; Soldatov, M.A.; Butova, V.V. Doxorubicin-Loaded Core-Shell UiO-66@SiO_2 Metal-Organic Frameworks for Targeted Cellular Uptake and Cancer Treatment. *Pharmaceutics* **2022**, *14*, 1325. [CrossRef]
68. Li, J. Chidamide Enhances Cytotoxicity of Doxorubicin by Promoting Autophagy and Apoptosis in Breast Cancer. *BMC Cancer* **2023**, *23*, 353. [CrossRef]
69. Alioghli Ziaei, A.; Erfan-Niya, H.; Fathi, M.; Amiryaghoubi, N. In Situ Forming Alginate/Gelatin Hybrid Hydrogels Containing Doxorubicin Loaded Chitosan/AuNPs Nanogels for the Local Therapy of Breast Cancer. *Int. J. Biol. Macromol.* **2023**, *246*, 125640. [CrossRef]